A&A 450, 181–192 (2006)
DOI: 10.1051/0004-6361:20054300

Astronomy & Astrophysics

Resolving the compact dusty discs around binary post-AGB stars using *N*-band interferometry⋆

P. Deroo[1], H. Van Winckel[1], M. Min[2], L. B. F. M. Waters[1,2], T. Verhoelst[1], W. Jaffe[3], S. Morel[4], F. Paresce[4], A. Richichi[4], P. Stee[5], and M. Wittkowski[4]

[1] Instituut voor Sterrenkunde, KU Leuven, Celestijnenlaan 200B, 3001 Leuven, Belgium
e-mail: Pieter.Deroo@ster.kuleuven.be
[2] Astronomical Institute "Anton Pannekoek", University of Amsterdam, Kruislaan 403, 1098 SJ Amsterdam, The Netherlands
[3] Leiden Observatory, PB 9513, Leiden 2300 RA, The Netherlands
[4] European Southern Observatory, Karl-Scharzschild-Strasse 2, 85748 Garching, Germany
[5] Observatoire de la Côte d'Azur, CNRS-UMR 6203, Avenue Copernic, 06130 Grasse, France

Received 4 October 2005 / Accepted 5 January 2006

ABSTRACT

We present the first mid-IR long baseline interferometric observations of the circumstellar matter around binary post-AGB stars. Two objects, SX Cen and HD 52961, were observed using the VLTI/MIDI instrument during Science Demonstration Time. Both objects are known binaries for which a stable circumbinary disc is proposed to explain the SED characteristics. This is corroborated by our *N*-band spectrum showing a crystallinity fraction of more than 50% for both objects, pointing to a stable environment where dust processing can occur. Surprisingly, the dust surrounding SX Cen is not resolved in the interferometric observations providing an upper limit of 11 mas (or 18 AU at the distance of this object) on the diameter of the dust emission. This confirms the very compact nature of its circumstellar environment. The dust emission around HD 52961 originates from a very small but resolved region, estimated to be ∼35 mas at 8 μm and ∼55 mas at 13 μm. These results confirm the disc interpretation of the SED of both stars. In HD 52961, the dust is not homogeneous in its chemical composition: the crystallinity is clearly concentrated in the hotter inner region. Whether this is a result of the formation process of the disc, or due to annealing during the long storage time in the disc is not clear.

Key words. stars: circumstellar matter – stars: AGB and post-AGB – stars: individual: HD 52961 – stars: individual: SX Cen – techniques: interferometric – infrared: stars

1. Introduction

The fast stellar evolution connecting the Asymptotic Giant Branch (AGB) to the Planetary Nebulae (PNe) phase is still poorly understood (e.g. Van Winckel 2003). Many detailed studies of individual transition objects (post-AGB stars) exist, but it is not clear how these objects are related by evolutionary channels. Moreover, there is general agreement that binary interactions must play a significant role in many well studied sources. Binarity is for instance invoked in the physical models to understand the observational characteristics of some spectacular geometries observed in PNe. More recently, also the geometries and kinematical structures around resolved post-AGB stars might be linked to binarity (Balick & Frank 2002, and references therein). Since many uncertainties remain in our understanding of the final evolution of single stars, it is no surprise that this is even more the case when the star is a member of a binary system.

Direct detection of the binary nature of central stars of resolved nebulae is often difficult due to the high obscuration. Moreover, in crossing the HR-diagram, the stars must pass the pop II Cepheid instability strip, in which pulsational instabilities occur. This makes radial velocity variations not a straightforward signature of orbital variations.

In the sample of optically bright post-AGB stars, binaries are being detected, however, and for an overview we refer to Van Winckel (2003, and references therein). One of the important observational characteristics of those binaries is the shape of their SED. They show a dust-excess starting near sublimation temperature, irrespective of the effective temperature of the central object and this despite the lack of a current dusty mass loss (De Ruyter et al. 2005b,c, and references therein). Moreover, when available, the long wavelength fluxes show a black-body slope which indicates the presence of a component of large mm-sized grains. It is argued in

⋆ Based on observations made with the Very Large Telescope Interferometer of the European Southern Observatory (program id 073.A-9002(A)), the 1.2 m Flemish Mercator telescope at Roque de los Muchachos, Spain and the 1.2 m Swiss Euler telescope at La Silla, Chile.

De Ruyter et al. (2005c) that in all the investigated objects, gravitationally bound dust is present, likely in a Keplerian disc. Note that only for the most famous example, the Red Rectangle, this dust emission is resolved and it shows a clear disc structure, both in the near-IR and in the visible (Men'shchikov et al. 2002; Cohen et al. 2004). Moreover, the gaseous component was spatially resolved using mm-interferometry (Bujarrabal et al. 2003, 2005). The latter observations clearly demonstrated the Keplerian rotation of the disc. In all other cases, the presence of a disc is postulated. More detailed studies of individual cases can be found: examples are 89 Her (Waters et al. 1993), HR 4049 (Waelkens et al. 1991a; Dominik et al. 2003) and IRAS 08544-4431 (Maas et al. 2003). Given the orbits detected so far, one of the conclusions is that it is clear that most binaries cannot have evolved along single star evolutionary tracks.

The high spatial resolution of the mid-IR instrument MIDI mounted on the VLTI interferometer of ESO makes this an ideal instrument to probe the circumstellar material around these binaries for two reasons: (i) the discs are likely compact so high spatial resolution measurements are needed to resolve the discs and (ii) the discs are shown to emit a significant part of their total luminosity in the *N*-band. We therefore carefully selected 2 binary post-AGB stars for which there is significant indirect evidence for the presence of a stable circumstellar dust reservoir. The data presented in this contribution are taken during Science Demonstration Time to illustrate the potential of MIDI coupled to the VLTI to study the compact circumstellar environment suspected in those evolved stars.

In Sect. 2, we introduce both objects and refine the orbital parameters published in our previous papers. The observational log is presented in Sect. 3 while the reduction of the interferometric dispersed fringes is reported in Sect. 4. We discuss our findings in Sect. 5 and come to our conclusions in Sect. 6.

2. HD 52961 and SX Cen: global characteristics

SX Cen and HD 52961, having both a spectral type F-G (Kholopov et al. 1999; Shenton et al. 1994; Waelkens et al. 1991b), are located in the pop II instability strip with SX Cen known as a very regular RV Tauri star with a period of 32.9 days, while HD 52961 shows a photometric periodicity of 72 days. They are members of the chemically anomalous post-AGB stars for which the photospheric abundances of the different elements are closely linked to their condensation temperature (Waelkens et al. 1991b; Van Winckel et al. 1992, 1995; Maas et al. 2002). Members of this class show higher photospheric abundances for chemical elements with a lower condensation temperature. In fact, HD 52961 is one of the most extreme examples of this class of objects. It is a highly metal-poor object ([Fe/H] = −4.8, Waelkens et al. 1991b) which has more zinc than iron in absolute (!) number ([Zn/Fe] = +3.1, Van Winckel et al. 1992). There is general agreement that this abundance pattern is caused by a chemical fractionation process caused by dust formation in the circumstellar environment. After decoupling of the gas and dust, reaccretion of the gas causes the observed abundance pattern. Waters et al. (1992) proposed a scenario in which the circumstellar dust is trapped in a stable disc. The occurrence of such a disc likely implies binarity for post-AGB stars. Indeed, radial velocity measurements proved that all the extremely depleted objects are binaries (Van Winckel et al. 1995). In the following we refine our previously published Spectral Energy Distribution (SED) as well as the orbital elements of both objects.

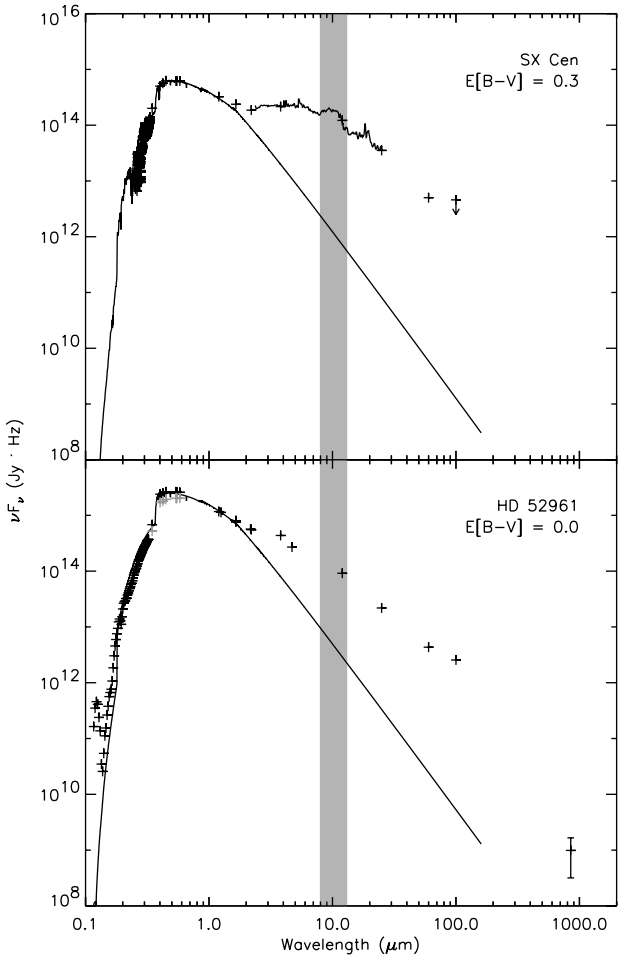

Fig. 1. The SED of both programme stars. On top, the SED of SX Cen is provided according to the parametrization given in the literature while at the bottom, the SED of HD 52961 is shown. The solid line is the scaled Kurucz model with stellar parameters determined in the literature ($T_{\rm eff}$ = 6500 K, log (g) = 1.5 and [Fe/H] = −1.0 for SX Cen, Maas et al. 2002; and $T_{\rm eff}$ = 6000 K, log (g) = 0.5 and [Fe/H] = −4.5 for HD 52961, Waelkens et al. 1991b). The photometric measurements are shown with plus symbols, black for photometric maximum, grey for photometric minimum. For SX Cen, the ISO/SWS spectrum is overplotted up to 25 μm. The MIDI wavelength range is indicated by a grey box.

2.1. Spectral energy distribution

The SED of SX Cen is discussed in the literature (Goldsmith et al. 1987; Shenton et al. 1994; Maas et al. 2002) where a total reddening of $E(B-V) = 0.3 \pm 0.1$ is found. They find a broad infrared excess starting already at K which, in combination with the confirmed binarity, is interpreted in Maas et al. (2002) as a signature of a dusty disc, not an outflow. The SED is reproduced in the top panel of Fig. 1 in which the ISO/SWS

spectrum is overplotted. This spectrum shows a broad silicate emission feature at 10 μm, inside the MIDI wavelength range. Due to the low flux levels at longer wavelengths, we cannot be conclusive about the origin of the feature around 18 μm. This is possibly an artifact, although it is present in both scans. The distance of SX Cen can be estimated comparing the intrinsic luminosity with the integrated flux of the scaled Kurucz model. The luminosity of SX Cen is estimated using the period-luminosity relation derived for the LMC RV Tauri variables (Alcock et al. 1998) to be about $600 \pm 400\ L_\odot$. The large uncertainty is a relic of the scatter in the *P-L* relation. This provides a rough distance estimate for SX Cen of 1.6 ± 0.5 kpc.

For HD 52961, we constructed a SED using IUE data (0.115 μm−0.320 μm), Geneva optical photometry, near-IR *JHKLM* photometry (Bogaert 1994) and far-IR IRAS photometry. In addition, one SCUBA (Holland et al. 1999) observation was made to obtain a continuum measurement at 850 μm, providing $F_{850\ \mu\mathrm{m}} = 2.8 \pm 1.9$ mJy with Mars as flux calibrator.

As the object suffers photometric variations over time, we constructed the SED for photometric maximum only. The colour excess due to interstellar and circumstellar extinction was estimated by searching the best correspondence between the appropriate Kurucz model and the dereddened SED in the optical and UV. The SED was dereddened using the average interstellar extinction law of Savage & Mathis (1979) and the Kurucz model was chosen according to the stellar parameters given in Waelkens et al. (1991b), i.e. $T_{\mathrm{eff}} = 6000$ K, $\log(g) = 0.5$ and [Fe/H] = −4.5. The result is shown in Fig. 1, where the Geneva photometry at photometric minimum is overplotted using grey crosses. While the photometry and the Kurucz model are consistent in the UV and optical, a clear IR excess due to dust is observed at longer wavelengths. This excess distribution, in combination with the confirmed binarity (Van Winckel et al. 1995, and refinements in Sect. 2.2) and the lack of a current dusty mass loss, is also interpreted as evidence for a dusty disc instead of an outflow. The luminosity of HD 52961 is estimated as $1900 \pm 1300\ L_\odot$ using the same period-luminisoty relation as for SX Cen, providing a distance of 1.4 ± 0.5 kpc.

In the MIDI wavelength range (8−13 μm), the amount of flux emitted by the stellar photosphere with respect to the total flux is only 1% for SX Cen and 5% for HD 52961. In addition, both objects show a clear silicate resonance in emission in the *N*-band (see the ISO/SWS spectrum in the top panel of Fig. 1 and the MIDI spectra in Fig. 4). Therefore, the MIDI instrument, providing spectrally dispersed visibilities over the *N*-band, is ideally suited to probe the circumstellar geometries of the dust around both objects.

2.2. Orbital elements

We refined the orbital elements which were published already in Van Winckel et al. (1999) and Maas et al. (2002) for HD 52961 and SX Cen respectively. Our accumulation of data is now such that we covered close to 3 (HD 52961) and 2 (SX Cen) orbital cycles. The heliocentric radial velocity data folded on the orbital periods are given in Fig. 2 and the orbital elements are listed in Table 1.

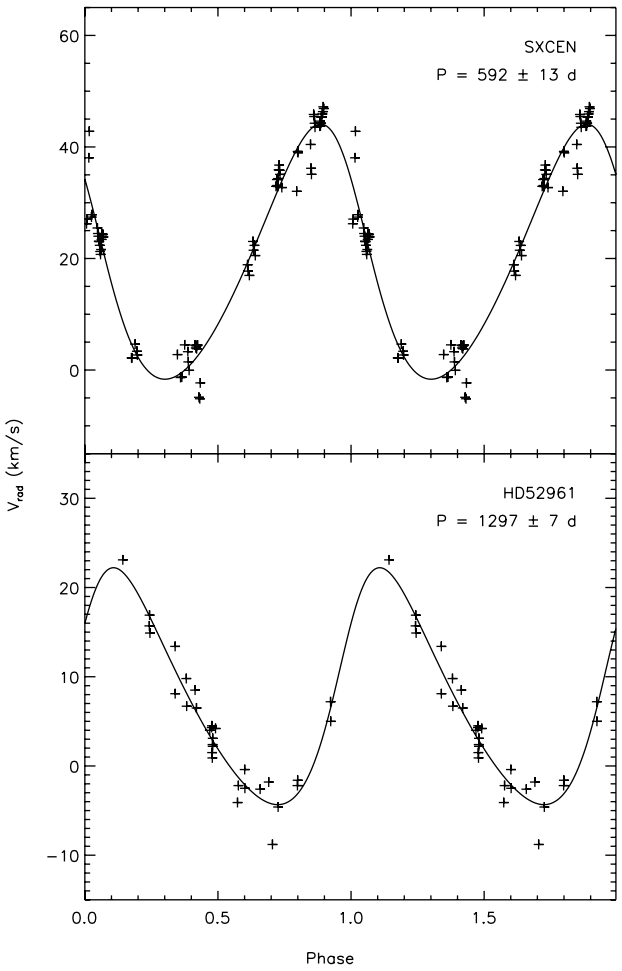

Fig. 2. The radial velocity curves of SX Cen and HD 52961 folded on their binary period. The data of SX Cen were cleaned from pulsationally induced variations as discussed in the text. The crosses are the measurements while the solid line is the orbital solution.

The data sampling of HD 52961 is not very extensive and in the residuals no clear modulation on the pulsational period is found. For the RV Tauri star SX Cen, the pulsational amplitude in radial velocity is significant. After pre-whitening of the orbital solution, the pulsational period of 16.46 d is clearly recovered (Fig. 3). We cleaned the original data with a harmonic least square fit of the 16.46 days pulsation period and three harmonics. The variance reduction of the pulsation model is 81%. After cleaning the original data with this pulsation model, we redetermined the orbital elements. The eccentric orbit was found to be significant according to the classical Lucy and Sweeney test (Lucy & Sweeney 1971).

As shown in our previous papers, both objects show a long term trend in their photometric light-curve which is due to variable circumstellar reddening in the line of sight towards the object. For SX Cen this long term trend is periodic with a period of 615 days (O'Connell 1933; Voûte 1940), very close to the orbital period. For HD 52961 it was not very clear whether the subtle effect is periodic or not.

If the circumstellar material is indeed mainly stored in a disc around the objects and assuming this disc is located in the orbital plane, the inclination of the disc cannot be very small.

Table 1. The orbital elements of the program stars. All symbols have their usual meaning. The number of measurements (N) and the number of covered orbital cycles in our monitoring program are also given.

	Unit	HD 52961	SX Cen
P	days	1297 ± 7	592 ± 13
T_0	JD	2 448 591 ± 38	2 452 107 ± 10
K	km s^{-1}	13.3 ± 0.9	22.9 ± 0.5
γ	km s^{-1}	7.4 ± 0.5	19.1 ± 0.4
e		0.22 ± 0.05	0.16 ± 0.02
$a \sin i$	AU	1.54	1.23
$f(M)$	$M_\odot$	0.29	0.70
N	#	31	78
cycles covered		2.9	2.0

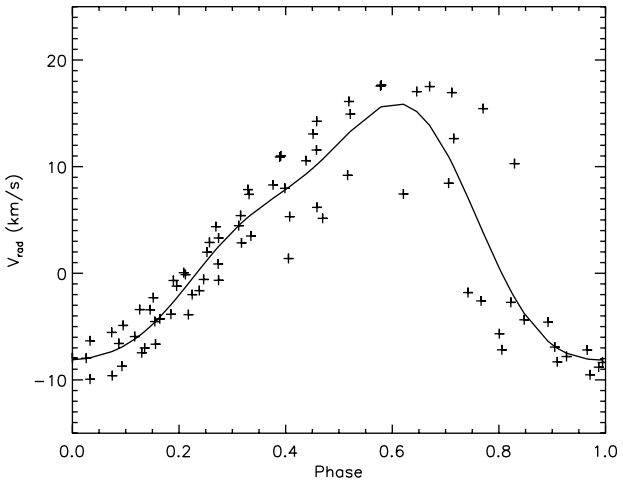

Fig. 3. The radial velocity variations induced by pulsation for SX Cen. The data indicated with crosses is pre-whitened with the orbital solution. The solid line is a harmonic least square fit of the 16.46 days pulsational period and three harmonics.

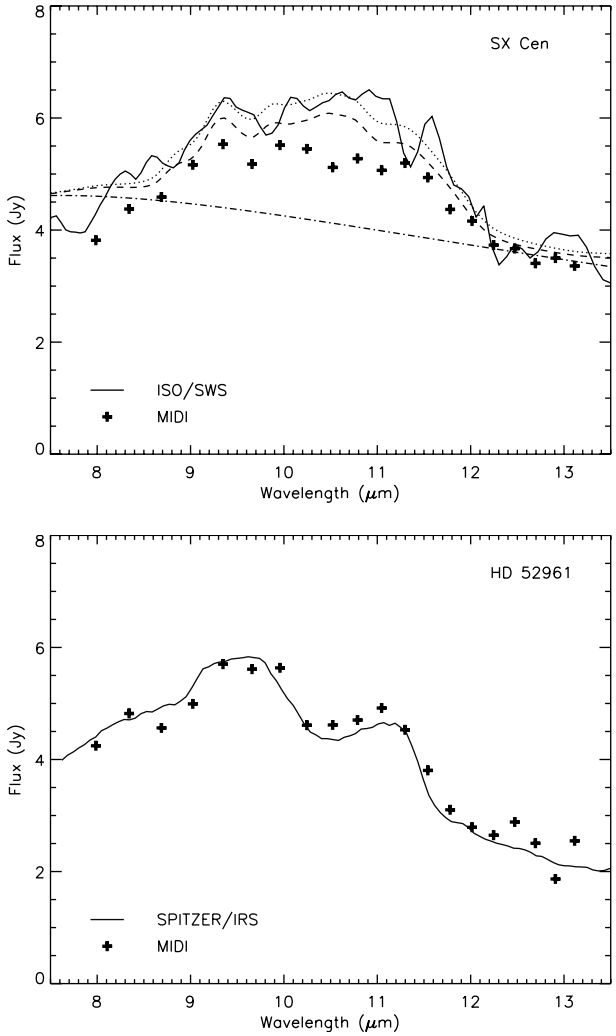

Fig. 4. The MIDI single telescope spectra of both programme stars are shown using black crosses. For the flux calibration, we only used the data of 10 February. In the upper panel (SX Cen), the full line shows the ISO/SWS spectrum. The dotted line is the result of our chemical model (Sect. 5.3), while the contribution of different individual dust components of the fit are given as well: the dashed-dotted line for the continuum and the dashed line for the crystalline component. In the lower panel, the full line shows the SPITZER/IRS spectrum of HD 52961.

Assuming an inclination varying between edge-on ($i = 90°$) up to 60°, and a mass of the evolved component of 0.6 $M_\odot$, the mass of the companion varies between 0.8−1.1 $M_\odot$ for HD 52961 and 1.4−1.9 $M_\odot$ for SX Cen. The unseen companion is probably an unevolved main sequence star, since the lack of an UV excess and of any sign of symbiotic activity make the presence of a massive compact object very unlikely. Moreover, the orbital characteristics in period and eccentricity make it very unlikely that the companion is a post red giant as well (Van Winckel 2003).

Neither stars are filling their Roche Lobe now, but in both cases it is clear that the actual orbit is too small to accommodate a full grown AGB star. The stars must have suffered an evolutionary phase with severe binary interaction when at giant dimensions.

3. Observations

The VLTI/MIDI interferometer (Leinert et al. 2003) was used to combine the light coming from the UT2 and UT3 telescopes. The observations of the targets, SX Cen and HD 52961, were performed in three nights of Science Demonstration Time in February at a projected baseline in the range of 40 to 50 meters. A detailed log of the observations of the science targets is presented in Table 2.

The following observing sequence was carried out, according to the standard procedures for MIDI, and repeated for target stars and calibrators. First, acquisiton images are obtained by both telescopes independently (i.e. without beam combiner and prism) to ensure overlap of the beams, which is required for interferometric combination. Then, the MIDI beam combiner, the slit and the prism are inserted. This produces two spectrally dispersed interferometric outputs of opposite phase. The zero optical path difference (OPD) is searched for by scanning a range of a few millimeters around the expected value. When found, MIDI uses its piezo-driven mirrors to keep the fringe pattern at a fixed position within a ≈200 μm scan length, while the VLTI delay lines compensate for the drift in OPD position due

Table 2. A summary of the observations with the MIDI instrument of SX Cen and HD 52961. For each science target, the calibrators used to calibrate the visibility are given (the flux calibrators are given in Table 3). The angular diameter in the Limb Darkened Disc approximation is obtained from Verhoelst (2005) (cf. `http://www.ster.kuleuven.ac.be/~tijl/MIDI_calibration/mcc.txt`). The reported flux for the calibrator sources is the IRAS 12.5 μm flux. Nomenclature: UT = Universal Time, PB = Projected Baseline and PA = Projected baseline Angle.

Night yyyy/mm/dd	Science target	UT hh mm ss	PB (m)	PA (°)	Airmass	Calibrator target	UT hh mm ss	Spectral type	Diameter (mas)	Flux (Jy)
2004/02/09	HD 52961	02 20 02	39.7	45	1.2	HD 49161	02 45 52	K4 III	2.44 ± 0.01	10.35
	SX Cen	07 37 52	44.6	41	1.1	HD 67582	06 24 15	K3 III	2.30 ± 0.01	9.33
						HD 67582	07 13 39	K3 III	2.30 ± 0.01	9.33
						HD 107446	08 08 53	K3.5 III	4.43 ± 0.02	32.42
2004/02/10	HD 52961	04 13 04	46.1	46	1.4	HD 67582	03 46 12	K3 III	2.30 ± 0.01	9.33
	SX Cen	07 37 52	44.6	41	1.1	HD 107446	08 16 44	K3.5 III	4.43 ± 0.02	32.42
2004/02/11	SX Cen	08 03 25	43.6	46	1.1	HD 120404	08 27 38	K7 III	2.96 ± 0.02	13.28

to sidereal motion and for the slow component of atmospheric piston. Fringes are integrated for about 1−3 min. Finally, photometric data are recorded using one telescope at a time, with the same optical set-up but using chopping to subtract sky and background.

To correct for optical imperfections and atmospheric turbulence, a calibrator of known diameter is measured as well. The time-lag between the measurement of this calibrator and the science object is about 30 min. However, considering the present accuracy per single visibility measurement of about 10%, we can also use calibrators observed in the same mode one or two hours earlier or later (see e.g. Leinert et al. 2004). A list of the calibrator observations is given in Table 2.

4. Reduction

4.1. Incoherent vs. coherent analysis

We used two different methods for the MIDI data reduction. The first method is based on power spectrum analysis (hereafter called incoherent analysis), while the second method reduces all frames to the same OPD and adds them coherently (hereafter called coherent analysis). For the incoherent analysis of the data, we used the MIA package (MIDI Interactive Analysis, `http://www.mpia-hd.mpg.de/MIDISOFT/`) developed at the Max-Planck Institut für Astronomie in Heidelberg, while for the coherent analysis we used the EWS package (Expert Work Station) developed by Walter Jaffe at the Leiden observatory (Jaffe 2004).

During the incoherent analysis, we separated the different scans in those with and without fringes, where each scan is Fourier-transformed from OPD to fringe frequency space. Considering the wavelengths present in the band and the rate at which the OPD is changing, the power is calculated in the correct frequency interval. The total power of all measured scans with fringes is then averaged and an estimate of the noise is subtracted. This noise estimate is based on the frames without fringes. This provides a value of the instrumental visibility squared of each channel. Contrary to the coherent method, the major difficulty of this method is that an accurate estimate of the off-fringe noise power is needed. Since our science targets have small fluxes in the 10 μm window, a reliable estimate of the noise power is difficult to obtain and we focused during data reduction on the coherent method (see below). Our incoherent analysis was only used to check the results obtained by a coherent analysis and both methods give consistent results.

4.2. Coherent analysis

We first investigated the photometric datasets. The averages of the target and sky frames are calculated and subtracted, providing a raw two-dimensional spectrum of the object. The position and width of this spectrum is determined and a spatial mask is constructed from the location and average width of the spectrum at each wavelength position. After multiplication of the detector images with this mask, the rows are added providing a one dimensional raw spectrum of the object (i.e. not corrected for the atmospheric transmission and instrumental efficiency).

The spatial mask is then used to extract the information of the interferometric observations as well, in the assumption that all instrumental parameters stay the same between the interferometric and photometric observation. The two detector spectra with opposite phase, are subtracted, resulting in one interferometrically modulated spectrum. In this way, the background is reduced by approximately 90 percent.

Contrary to the incoherent method which allows the summing of scans where the relative OPD is not known, the coherent method needs an accurate determination of the atmospheric delay. The large wavelength coverage of the *N*-band ensures that this can be accurately done by measuring the fringes in frequency space (rather than in OPD space which is done in an incoherent analysis, e.g. Tubbs et al. 2004). As a first step, the known instrumental delay is removed from each frame after which the (previously unknown) atmospheric delay is retrieved using a group delay estimation. At this point, the data is not yet fully coherent because of the instrumental phase imposed on the data (e.g. the varying index of refraction of water vapor imposes variations in phase that are not removed by a group delay fitting). These phase shifts are almost constant as a function of frequency and can be approximated as a constant phase shift over the *N*-band (Jaffe 2004). Finally, the data can be added coherently to obtain the final visibility amplitude and differential phase.

The instrumental visibility is then calculated dividing the fringe amplitude by the non-interferometric, photometric

Table 3. A summary of the calibrators used to flux calibrate the spectrum of SX Cen and HD 52961. All calibrators listed were observed on February, 10. The reported flux is the IRAS 12.5 μm flux, and the diameters are taken from Verhoelst (2005).

Calibrator target	UT hh mm	Airmass	Spectral type	Diameter (mas)	Flux (Jy)
HD 67582	02 37	1.09	K3 III	2.30 ± 0.01	9.33
HD 67582	03 46	1.07	K3 III	2.30 ± 0.01	9.33
HD 49161	04 43	1.56	K4 III	2.44 ± 0.01	10.35
HD 107446	08 16	1.24	K3.5 III	4.43 ± 0.02	32.42

exposures. Repeating this procedure for a calibrator enables to estimate the instrumental visibility loss and thus determining the calibrated visibility of the science object.

4.3. The data

4.3.1. Photometry

A raw spectrum is obtained each night by subtracting the masked target frames from the masked sky frames. This spectrum is flux calibrated and corrected for atmospheric transmission using the calibrator spectra observed during the same night. For the calibrators, the intrinsic spectra were synthetised from MARCS atmosphere models (Gustafsson et al. 1975, and further updates), using the temperature, surface gravity and angular diameter determined in van Boekel (2004). This approach is preferred over a Rayleigh-Jeans approximation of the calibrator spectrum, since the SiO first overtone band head is not negligible in a K giant N-band spectrum. The 12 μm flux of this synthetic spectrum is well within 1σ of the color corrected IRAS 12 μm flux. For both objects, the absolute flux calibration has been performed with the data of 10 February only, using the calibrators listed in Table 3. Both reduced spectra ($R \sim 30$) are shown in Fig. 4, where they are compared to independent spectra taken by the ISO/SWS ($R \sim 248$) and the SPITZER/IRS ($R \sim 127$) instrument.

4.3.2. Interferometry

We start this discussion with an error estimate on the observed visibilities. The main source of error is the varying overlap between the interferometric beams due to imperfect source acquisition and residual image motion (see e.g. Leinert et al. 2004). This reduces the visibility for calibrator and/or science object with an unknown amount. The shape over the N-band, however, remains the same. The visibility variation within the spectral band, is therefore much more reliable than its absolute value.

To get a quantitative estimate of the absolute uncertainty on the visibility, we look at all calibrators (∼point sources) observed during one night. If the interferometric efficiency is constant throughout the night, all calibrator measurements should yield the same instrumental visibility. In Fig. 5, the mean instrumental visibility of all six calibrators observed in the prism mode during the night of February 9 is plotted. The variance on the mean is overplotted. It is clear from this figure that the instrumental loss of visibility is much higher at 8 μm than at 13 μm and that the uncertainty on the absolute value of the visibility is about 15%. However, when calibrating the visibility of the science source using a calibrator source observed in direct concatenation, this quantitative error is an upper limit. In the following, we use an error of 15% on the absolute visibility, which is therefore a conservative estimate.

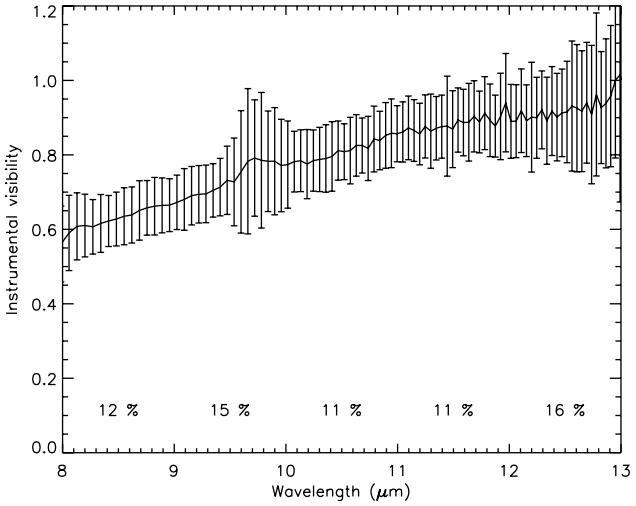

Fig. 5. The mean instrumental visibility of the six calibrators taken in prism mode on February 9. The variance on the mean is overplotted and for each wavelength interval of 1 μm, the mean variance is written below. The variance gives an estimate of the absolute error on the visibility, however the relative visibility is more reliable (∼5%).

Calibrated visibilities are obtained dividing the raw visibility by the instrumental visibility. To calibrate the measurement of SX Cen observed at 9 February, we used the mean instrumental visibility as obtained from the three last calibrator measurements. Unfortunately, such a mean could not be used for the other measurements. Instead, we employed the calibrator closest in time to calibrate the visibility of the science source (see Table 2). The resulting calibrated visibilities are shown in Figs. 6 and 7.

5. Discussion

5.1. Visibilities

Because the angle between the projected baselines is the same to within 5 degrees for both objects, no large effects due to a possible asymmetry in the source morphology are expected. Therefore, as a first-order approximation, we modelled the circumstellar environment of objects using a uniform disc. The visibility in this assumption is given by $V = 2J_1(x)/x$, where $x = 2\pi\theta B/\lambda$ with θ the diameter of the disc and B the projected baseline length. This function is smoothly increasing with wavelength, as long as $x < 1.22\pi$. The increase is however different for various amounts in resolving power, a steeper increase is observed if the source is more resolved. Assuming a temperature distribution in the disc, with the colder dust located further away from the star than the hotter dust, the gradient decreases. For an unresolved source, the value of the visibility remains constant at unity.

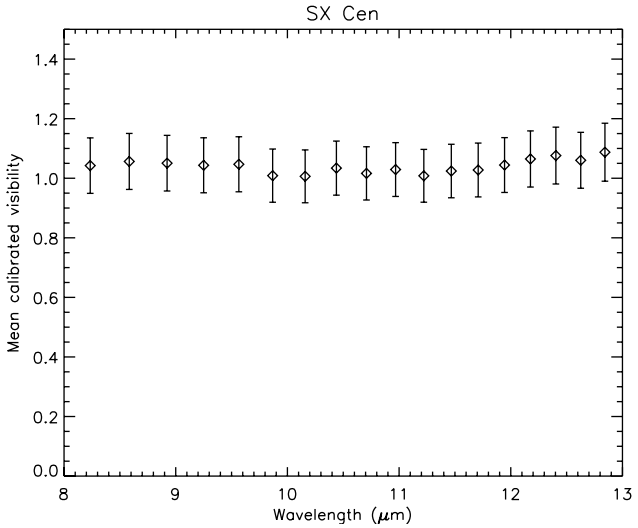

Fig. 6. The mean calibrated visibility of SX Cen. The value close to unity and the flatness of the profile over the passband show that SX Cen is unresolved at the particular orientation and baseline setting.

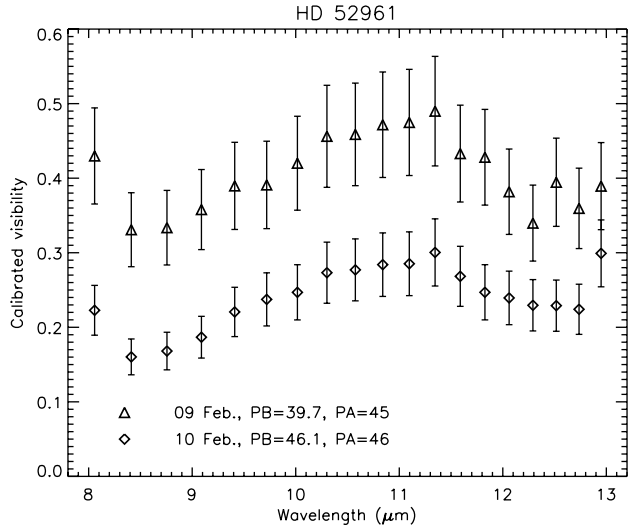

Fig. 7. The calibrated visibilities for HD 52961 as obtained in both measurements. The projected baseline (PB) is given in meters and the projected angle (PA) in degrees. Different symbols were used for both measurements.

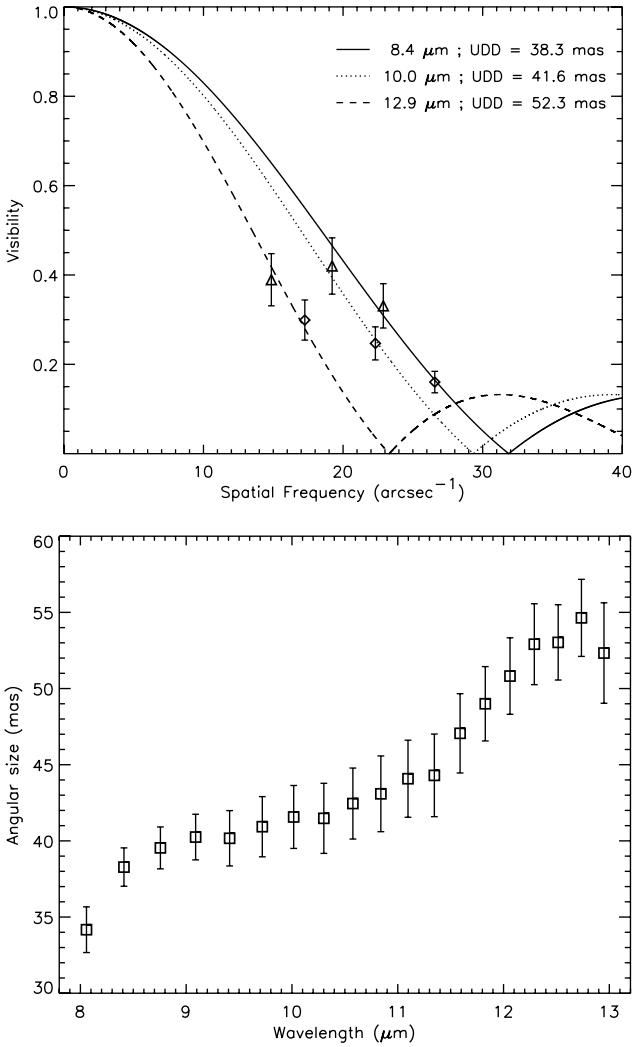

Fig. 8. *Upper panel*: the uniform disc fit to the data for three different wavelength bins. The lines in the plot are the uniform disc models with different sizes while the symbols are the measurements. Triangles were used for the measurements of 9 February while diamonds were used for those of 10 February. *Lower panel*: the angular size of the dust around HD 52961 as determined using a uniform disc model for each wavelength bin.

The disc around SX Cen is unresolved in all measurements even using a 45 m baseline. The visibility is close to unity and shows a flat distribution over the passband. The mean calibrated visibility for all measurements is shown in Fig. 6. Because all measurements are observed at approximately the same projected angle (ranging from 41 to 46 degrees) this means that in that particular orientation, the structure is smaller than 11 mas at 8 μm and 17 mas at 13 μm in a uniform disc approximation. Using a Gaussian distribution modelling, the FWHM gives respectively 7 mas and 10 mas as upper limits.

HD 52961 shows quite a different picture. For this source, the visibilities are low (see Fig. 7), thus the source is clearly resolved. Immediately noted is the fact that we do not get an increase in visibility amplitude which is quite linear (expected for a uniform disc model in the observed visibility range). Instead we see a "bump" in the visibility pattern ranging from 9 to 12 μm. The geometry of the disc around this object can clearly not be modelled with the same uniform disc at all wavelenghts (see also Fig. 8). Using a uniform disc approximation for each wavelength independently is however instructive. For each wavelength bin, we made a χ^2 minimalisation between the observed visibility at both baselines and a uniform disc model. This fit is shown for three representative wavelengths in the upper panel of Fig. 8. The diameter of the source at all wavelength bins in a uniform disc approximation is shown in the lower panel of Fig. 8. The measurements at both baselines are very consistent in a uniform disc approximation for each wavelength independently (the mean reduced chi-square over the wavelength band is as low as 0.09) and provide a diameter increasing from ~35 mas at 8 μm to about ~55 mas at 13 μm. In a Gaussian distribution modelling, the FWHM gives

respectively ~23 mas and ~34 mas (and a mean reduced chi-square of 0.22). The increase towards longer wavelengths is consistent with a dust-distribution for which the temparture decreases further away from the star. We however note that the observed increase in size is not smooth over the wavelength band. There is an increase in size from 8 μm to 8.5 μm and onwards 11.5 μm, while in between a sort of plateau exists. We interpret this plateau as resulting from a non-homogenous distribution of the radiating silicates which contribute most in the inner regions close to the central star, thus lowering the overall size (see also the following sections).

For both objects we interpret the small angular scales of the dust around the objects as another clear indication that the circumstellar dust is stored in a compact Keplerian disc around the system.

5.2. Spectra

The SED of both objects shows a significant near-IR excess, indicative of a hot dust component, while there is no evidence for an ongoing dusty mass loss of those rather hot stars. In De Ruyter et al. (2005c), this is interpreted as originating from a hot inner rim near dust sublimation temperature. Because no dust can survive at higher temperatures, this dust receives head on radiation from the star and is therefore supposed to be puffed up (e.g. the wall model for HR4049 elaborated by Dominik et al. 2003). This is corraborated by the lower limit on the opening angle of the disc as seen from the star of 13° for HD 52961 and 32° for SX Cen (De Ruyter et al. 2005c). In this model, we expect a highly centerally peaked intensity distribution which provides that the correlated spectra measured by the interferometer are dominated by the inner regions of the disc. However, because of the varying spatial resolution from 8 to 13 μm, a slope is introduced in the correlated spectrum. To determine the magnitude of this effect, a detailed modelling has to be performed, which is out of the scope of this article. For now, we assume that this effect is a smooth function of wavelength, thus having only a marginal effect on any mineralogy determination.

Because SX Cen is unresolved at all employed baseline settings, the correlated spectrum is identical to the single telescope spectrum and thus no additional information is available for this object. However, for HD 52961, which is clearly resolved in both measurements, the shape of the two correlated spectra is predominantly determined by the inner parts of the disc. This means that we can construct independent spectra of geometrically different areas of dust around HD 52961. The single telescope spectrum provides the full *N*-band spectrum of all the dust around HD 52961. The correlated spectra sample smaller parts of the disc. These spectra, each sampling a different geometrical part of the disc, are shown in Fig. 9. From this figure, it is clear that the shape of the correlated spectra is quite different from the single telescope spectrum. This points to a different chemical composition of the inner part of the disc and the outer part of the disc. To quantify this, we have fitted the different spectra independantly.

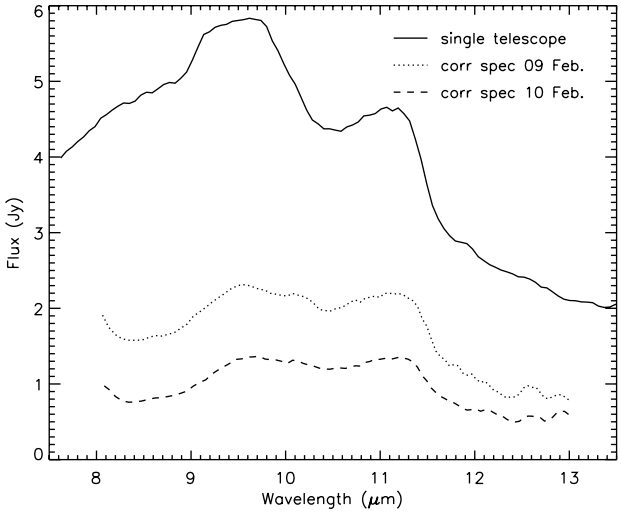

Fig. 9. The spectra of different parts of the dust around HD 52961. The solid line is the single telescope spectrum sampling all the dust around HD 52961. The dotted and dashed line give the spectrum of smaller parts of the disc around the object, namely the unresolved part of the disc in each measurement.

Table 4. A list of the references of the complex refractive indices employed for the various grain species.

Grain species	Reference
Amorphous Olivine	Dorschner et al. (1995)
Amorphous Pyroxene	Dorschner et al. (1995)
Forsterite	Servoin & Piriou (1973)
Enstatite	Jäger et al. (1998)
Amorphous Silica	Spitzer & Kleinman (1960)

5.3. Silicate mineralogy

In order to determine the mineralogy and sizes of the emitting dust grains, we made a fit to the *N*-band spectra using calculated emissivities of irregularly shaped, chemically homogeneous dust grains. The most important dust species causing spectral signature in the 10 μm window are amorphous and crystalline olivine ($Mg_{2x}Fe_{2-2x}SiO_4$), amorphous and crystalline pyroxene ($Mg_xFe_{1-x}SiO_3$), and amorphous silica (SiO_2), where x determines the Mg/Fe ratio ($x = 1$ for the crystalline silicates, $x = 0.5$ for the amorphous silicates). The complex refractive indices for the different grain species were taken from various authors listed in Table 4. To simulate the effects of particle irregularity we employ a particular implementation of the so-called *statistical approach* using a distribution of hollow spheres. This distribution is very successful in reproducing the measured absorption spectra of irregularly shaped particles (Min et al. 2003, 2005). In addition to the dust species causing the feature, we also add a continuum contribution which accounts for emission by large grains and/or for the possible presence of featureless components such as metallic iron and iron sulfide. This continuum contribution is modeled using a constant mass absorption coefficient. In the 10 μm region we are mainly sensitive to the dust grains smaller than a few μm. We represent the size distribution of the particles by two different grain sizes, 0.1 and 1.5 μm. A similar method

Table 5. The composition and grain sizes of the dust in the circumstellar environments around SX Cen and HD 52961 as derived from our fitting procedure. The olivine and pyroxene grains are amorphous while the forsterite and enstatite are crystalline. For HD 52961 56% of the dust mass is in the inner disk region. It should be noted that, as explained in the text, the temperatures determined for the inner and outer disc spectra of HD 52961 are not realistic.

Star	T_c	Cryst.	Large	Olivine [%]		Pyroxene [%]		Forsterite [%]		Enstatite [%]		Silica [%]	
	10^2 K	[%]	grains [%]	Small	Large	Small	Large	Small	Large	Small	Large	Small	Large
SX Cen	$6.8^{+0.3}_{-0.3}$	78^{+17}_{-23}	93^{+3}_{-4}	–	21^{+24}_{-17}	–	1^{+6}_{-1}	7^{+3}_{-3}	25^{+9}_{-9}	–	46^{+12}_{-15}	1^{+1}_{-1}	0^{+2}_{-0}
HD 52961 (inner)	12^{+2}_{-2}	79^{+10}_{-12}	63^{+7}_{-12}	6^{+13}_{-6}	4^{+16}_{-4}	–	1^{+15}_{-1}	31^{+3}_{-3}	1^{+7}_{-1}	0^{+6}_{-0}	47^{+9}_{-11}	–	9^{+3}_{-3}
HD 52961 (outer)	14^{+1}_{-1}	19^{+4}_{-3}	59^{+18}_{-17}	–	5^{+10}_{-5}	22^{+16}_{-17}	20^{+19}_{-16}	19^{+3}_{-3}	–	–	0^{+4}_{-0}	0^{+1}_{-0}	34^{+4}_{-3}

was successfully employed by, for example, Bouwman et al. (2001), Honda et al. (2003), Honda et al. (2004), van Boekel et al. (2004) and van Boekel et al. (2005) to fit 10 μm emission spectra of circumstellar discs. Particles larger than a few μm contribute mainly to the continuum. In addition we assume that the thermal radiation we analyze originates from optically thin parts of the disc, which allows us to add the contributions from the various components linearly. For the emission of the outer parts of the disc, tentatively attributed to layers directly heated by the stellar flux, this is a reasonable approximation. Because the stellar radiation is incident under a high inclination, the temperature distribution in the surface layer of the disc must be very sharp and therefore, the emission in the *N*-band comes likely from optically thin parts. For the inner parts of the disc, the situation is more complex: a large fraction of the radiation comes from the inner rim, which has regions of both low and high opacity. The fit, using an optically thin assumption for the different contributing minerals, is therefore certainly too simplistic. We use it here as a first order estimate to show the chemical gradient of the silicates in the disc, but a detailed 2D radiative transfer model with a gradient in the physico-chemical condition of the dust grains will be needed to quantify the results. This is outside the scope of this paper.

We assume all dust grains, including the ones causing the continuum, to have the same temperature distribution. Due to the limited wavelength range this temperature distribution can be represented by a single Planck curve with a characteristic temperature T_c. This is justified because it is very likely that the dust grains of different species are coagulated, implying thermal contact between the various components. The characteristic temperatures used in the modeling are given in Table 5.

The abundances of the dust components are determined by using a linear least square fitting procedure with constraints on the weights to avoid negative values. The temperature of the grains and the underlying continuum is varied from 0 to 1500 K until a best fit is obtained.

The dust parameters derived from the unresolved spectrum of SX Cen are given in the upper row of Table 5. The resulting best fit spectrum is shown as a dotted line in Fig. 4. The grains in the circumstellar environment of SX Cen are highly crystalline and also on average relatively large compared to the interstellar grain population. This implies a large amount of dust processing in the circumstellar environment.

For HD 52961, we fit the spectrum corresponding to the inner disk (the correlated spectrum, angular size ~20 mas) and that corresponding to the outer disk (the total disk spectrum from which the correlated spectrum is subtracted) separately. We focus here on the correlated spectrum taken with the 40 m baseline. The resulting best fit model spectra are shown in Fig. 10 and the composition is given in Table 5. The varying spatial resolution over the *N*-band introduces an extra slope in the spectra which was not corrected. Therefore,

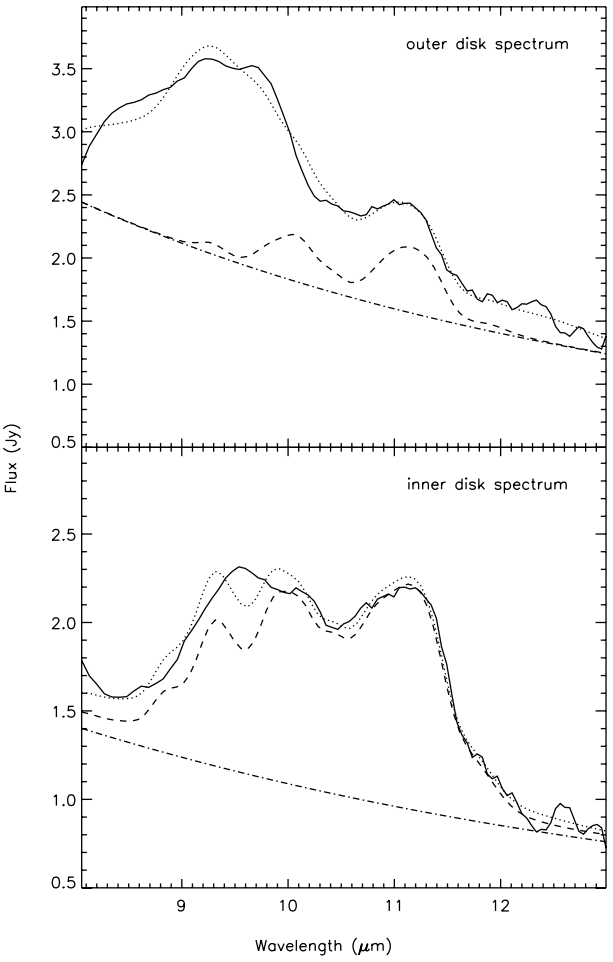

Fig. 10. The *N*-band spectrum of the outer disc (*top panel*) and the inner disc (*bottom panel*) of HD 52961, as obtained using a projected baseline of 40 m, are shown using solid lines. The best fit models of these spectra are overplotted using a dotted line. The continuum and the emission produced by crystalline particles are represented using a dashed-dotted and a dashed line respectively. For these models, the detailed information is given in Table 5. It is clear that the hot inner part of the disc is much more crystalline than the outer parts.

the characteristic temperatures (T_c) derived for the inner and outer disc spectra are not realistic. The influence of this slope on the determined chemical fractions is however expected marginal (see e.g. van Boekel et al. 2004). The average composition over the disk can be derived by taking the mass weighted average of the inner (56%) and outer (44%) disk regions. The overall composition of the dust in HD 52961 is for ~50% crystalline, and contains ~60% 1.5 μm grains. This is considerably less than what we find in SX Cen. It is also clear from Table 5 that the crystalline silicates are not uniformly distributed over the disk. The inner disk has a much higher crystallinity than the outer disk.

In order to fit the prominent feature around 9.5 μm in the total and the outer disk spectra of HD 52961, we have to add large (1.5 μm) silica grains. We have tried several other dust components in order to explain this spectral feature, but found no spectral match using any of them. We have no explanation for the presence of these amounts of large silica grains, and thus its detection is debatable. However, its presence is also indicated from the Spitzer IRS spectrum, which shows a weak feature around 21 μm which is naturally reproduced using large silica grains (not shown). For a full mineralogy, the broader wavelength range sampled by our Spitzer data is needed which is outside the scope of this paper.

5.4. Formation history of the disc

The composition of the dust in the circum-binary disc as a function of distance from the binary can give important clues to its formation history. In principle, the disc could have been formed by capturing a "normal" AGB wind, or through non-conservative mass transfer in an interacting binary. In the wind scenario, it is not unreasonable to assume that most dust was in the form of amorphous silicates, since this is the usual dust composition for O-rich AGB stars with a moderate to high mass loss rate (see e.g. Sloan & Price 1995; Waters et al. 1996; Cami 2002). In the interacting binary scenario, the dust may or may not have formed before the material entered the circum-binary disc, but in any case the thermal history of that dust would have been very different from that of the wind scenario: the grains were likely at high temperatures for a long period of time, increasing the chances of a substantial crystallisation. Therefore the wind scenario predicts a predominantly amorphous silicate composition, while the interacting binary scenario more likely produces (highly) crystalline discs.

Once in the disc, both grain aggregation and crystallisation may occur. Grain aggregation is a strong function of density and thus would be most efficient in the inner disc regions. Large grains settle quickly to the mid-plane thus creating a cold mid-plane population of grains, which we believe is responsible for the millimeter continuum emission (see e.g. De Ruyter et al. 2005c). The inner disc reaches temperatures above the glass temperature, forcing the grains to anneal. Therefore, in both the wind and in the interacting binary scenarios the innermost disc regions are expected to be strongly crystalline. The two scenarios predict strongly differing radial gradients in crystallinity however.

The present-day orbital parameters of the binary systems with circum-binary discs strongly suggest that interaction took place when the current post-AGB star was on the AGB. Therefore it seems difficult to imagine that a standard stellar wind formed the discs, and one would expect the discs on average to have much higher crystallinity than typical AGB winds. The recent spectral survey by De Ruyter et al. (2005a) indeed suggests that the circumbinary discs are much more crystalline than typical AGB outflows. One complicating factor is that at present not much is known about the composition of the dust in AGB outflows in the dust forming layers: by far most data are spatially unresolved and present the final outcome of the dust formation process in O-rich AGB outflows.

Our MIDI observations indeed confirm that the inner disc region of HD 52961 is extremely crystalline, and that the outer disc regions are less so. At first glance this would suggest the wind scenario is more likely, but the orbital parameters indicate substantial AGB interaction. These first MIDI observations thus raise interesting questions: is the outer disc of HD 52961 really amorphous and what kind of disc formation scenario could lead to amorphous grains? Does this hold for all systems, or is there an orbital separation dependence? Clearly more study is required to answer these questions.

5.5. Comparison with Herbig Ae/Be stars

In De Ruyter et al. (2005c), it is argued that the broad-band SED characteristics of the discs around binary post-AGB objects are very similar to the those of the Herbig Ae/Be group II sources. Herbig Ae/Be stars are intermediate mass pre-main sequence stars surrounded by remnant material of the star formation process. For these objects, the existence of a passive circumstellar disc is firmly established (e.g. Waters & Waelkens 1998; Eisner et al. 2003, and references therein). The Herbig Ae/Be stars are subdivided in two groups (Meeus et al. 2001) with the group I sources showing a rising mid-IR flux excess, while the group II sources only show a modest mid-IR excess. The difference in SED characteristics between both groups is attributed to disc geometry. The mid-IR excess of group I sources is indicative of the flaring of the outer disc, while the inner rim of the group II sources shadows the whole disc and no flaring occurs (Chiang & Goldreich 1997; Dullemond et al. 2001). van Boekel (2004) used the most recent models (Dullemond & Dominik 2004) of the discs around Herbig Ae/Be stars to compute the visibilities to be expected in the MIDI wavelength range. Leinert et al. (2004) on the other hand made observations with the MIDI instrument of several of these objects. We make a comparison of the results obtained in these publications for the group II sources and our observations under the assumption of the similarity of both source geometries.

Concerning the continuum radiation, the modelling performed in van Boekel (2004) shows that the size of the disc increases more rapidly from 8 to 13 μm than the interferometric resolution decreases. This provides a visibility curve which is decreasing from 8 to 13 μm. The observations indeed show this qualitative behaviour, however some objects, e.g. HD 144432,

show a rather horizontal slope. This very similar behaviour is observed for HD 52961 as well. The slope of the continuum visibility does not increase as expected for a uniform disc, it is instead rather constant with wavelength.

Concerning the visibility in the feature, the modelling performed by van Boekel (2004) suggests a lowered visibility for the silicate feature than for the continuum. The disc is irradiated by the central object and therefore the disc surface is hotter than the disc midplane. Because the opacity in the silicate resonance band is higher than in the continuum, one looks less deep into the disc in the resonance. This results in the fact that in the 10 μm region, a larger region in the resonance is seen than in the continuum. The observations of Herbig Ae/Be stars show a similar qualitative behaviour, however the visibility decrease is less pronounced. In fact, van Boekel et al. (2004) finds that for three Herbig Ae stars of the sample of Leinert et al. (2004), there is a large radial gradient in the processing. The innermost region of the proto-planetary discs has a substantially higher crystallinity degree with a shape very similar to that of comets in our solar system, while the outer region is clearly less processed. Clearly, the homogenous distribution of dust adopted in the modelling of these discs is a very crude approximation. For HD 52961, no visibility decrease is observed in the feature, instead an increase is seen. The spatial distribution of the dust responsible for the resonance is not homogeneously distributed, instead the hot inner region of the dust is much more crystalline than the outer parts (Sect. 5.3). This qualitative similarity in the distribution of the chemical species in the discs around some Herbig Ae stars and HD 52961 is surprising in the context of the completely different formation history of both.

6. Conclusions

The main conclusion of our presented MIDI observations is that they prove the very compact nature of the circumstellar environments of HD 52961 and SX Cen. SX Cen is not resolved using a 45 m baseline, which gives an upperlimit of only 18 AU at the estimated distance. For the well resolved HD 52961, the angular size in the *N*-band varies between 35 and 55 mas in a uniform disc approximation, which translates to a size of 50 and 80 AU.

Both stars have an effective temperature in the 6000 K range and since there is no evidence for a current dusty mass-loss we interpret these results as a very stringent proof of the existence of a stable reservoir near the star. A Keplerian disc seems the only plausible solution. The dust sublimation temperature is reached much further out than the binary orbits, hence the discs must be circumbinary. This is corroborated by the measured size of the dust-emission region around HD 52961.

Given the size of the orbits, the discs were probably formed in a poorly understood phase of strong binary interaction, when the star was at giant dimensions. Both discs are O-rich and there is no evidence for a C-rich component. They were consequently formed prior to the late AGB evolution where the stars could have changed into C-stars. The mass of the companion of SX Cen (1.4−1.9 $M_{\odot}$) is probably within the range of C-star progenitors. We conclude that the normal single star AGB evolution was shortcut by the presence of a binary companion. Clearly the formation of a stable Keplerian disc is a key ingredient in the late evolution of both binaries.

SX Cen is an RV Tauri star of photometric class b which shows a long term variability of the mean magnitude with a period similar to its orbital period probably due to variable circumstellar extinction in the line of sight during orbital motion. The inclination cannot be very small. Additional interferometric data on different projected angles will be necessary to probe the expected asymmetries.

The characteristics of the dust grains seem to be very different from normal single star outflows. This is shown in the mineralogy of the silicate resonance feature which shows for both objects a highly crystalline component and a size distribution with a much stronger component of large (>1 μm) grains than what is observed in outflows of AGB stars. It is not clear whether this reflects the formation history of the disc or this is due to the longer processing time of the dust in the Keplerian discs. Our analysis of HD 52961 shows that the crystallinity is clearly concentrated in the hotter inner region of the disc. Crystallisation by annealing is very temperature dependent and a similar picture arises as what is seen in the discs around some young stellar objects: the grains in the hot inner region were subject to a much stronger processing while in the outer region remained less processed. MIDI as spectrally dispersed *N*-band interferometer is an ideal instrument to study the chemo-physical structure of the inner regions of these discs.

Acknowledgements. The authors would like to thank Jeroen Bouwman for the reduction of the SPITZER/IRS spectrum of HD 52961 and Bram Acke for the reduction of the ISO/SWS spectrum of SX Cen. We also like to thank the referee, K. Ohnaka, for the many valuable comments. We thank the staff of the Geneva Observatory and the staff of the Instituut voor Sterrenkunde of the KU Leuven for the generous award of time on the Swiss Euler telescope at La Silla and the Flemish Mercator telescope at La Roque de los Muchachos respectively. We also thank our colleagues from the Instituut voor Sterrenkunde for their contribution to the gathering of the data. P.D. and H.V.W. acknowledge financial support from the Fund for Scientific Research of Flanders (FWO).

References

Alcock, C., Allsman, R. A., Alves, D. R., et al. 1998, AJ, 115, 1921
Balick, B., & Frank, A. 2002, ARA&A, 40, 439
Bogaert, E. 1994, Ph.D. Thesis
Bouwman, J., Meeus, G., de Koter, A., et al. 2001, A&A, 375, 950
Bujarrabal, V., Neri, R., Alcolea, J., & Kahane, C. 2003, A&A, 409, 573
Bujarrabal, V., Castro-Carrizo, A., Alcolea, J., & Nerii, R. 2005, A&A, submitted
Cami, J. 2002, Ph.D. Thesis
Chiang, E. I., & Goldreich, P. 1997, ApJ, 490, 368
Cohen, M., Van Winckel, H., Bond, H. E., & Gull, T. R. 2004, AJ, 127, 2362
De Ruyter, S., Van Winckel, H., & Dejonghe, H. 2005a, A&A, in prep.
De Ruyter, S., Van Winckel, H., Dominik, C., Waters, L. B. F. M., & Dejonghe, H. 2005b, A&A, 435, 161
De Ruyter, S., Van Winckel, H., Maas, T., Lloyd Evans, T., & Dejonghe, H. 2005c, A&A, submitted

Dominik, C., Dullemond, C. P., Cami, J., & van Winckel, H. 2003, A&A, 397, 595
Dorschner, J., Begemann, B., Henning, T., Jäger, C., & Mutschke, H. 1995, A&A, 300, 503
Dullemond, C. P., & Dominik, C. 2004, A&A, 417, 159
Dullemond, C. P., Dominik, C., & Natta, A. 2001, ApJ, 560, 957
Eisner, J. A., Lane, B. F., Akeson, R. L., Hillenbrand, L. A., & Sargent, A. I. 2003, ApJ, 588, 360
Goldsmith, M. J., Evans, A., Albinson, J. S., & Bode, M. F. 1987, MNRAS, 227, 143
Gustafsson, B., Bell, R. A., Eriksson, K., & Nordlund, A. 1975, A&A, 42, 407
Holland, W. S., Robson, E. I., Gear, W. K., et al. 1999, MNRAS, 303, 659
Honda, M., Kataza, H., Okamoto, Y. K., et al. 2003, ApJ, 585, L59
Honda, M., Kataza, H., Okamoto, Y. K., et al. 2004, ApJ, 610, L49
Jaffe, W. J. 2004, in New Frontiers in Stellar Interferometry, Proc. SPIE, 5491, ed. W. A. Traub., Bellingham, WA: The International Society for Optical Engineering, 715
Jäger, C., Molster, F. J., Dorschner, J., et al. 1998, A&A, 339, 904
Kholopov, P. N., Samus, N. N., Frolov, M. S., et al. 1999, VizieR Online Data Catalog, 2214, 0
Leinert, C., Graser, U., Przygodda, F., et al. 2003, Ap&SS, 286, 73
Leinert, C., van Boekel, R., Waters, L. B. F. M., et al. 2004, A&A, 423, 537
Lucy, L. B., & Sweeney, M. A. 1971, AJ, 76, 544
Maas, T., Van Winckel, H., & Waelkens, C. 2002, A&A, 386, 504
Maas, T., Van Winckel, H., Lloyd Evans, T., et al. 2003, A&A, 405, 271
Meeus, G., Waters, L. B. F. M., Bouwman, J., et al. 2001, A&A, 365, 476
Men'shchikov, A. B., Schertl, D., Tuthill, P. G., Weigelt, G., & Yungelson, L. R. 2002, A&A, 393, 867
Min, M., Hovenier, J. W., & de Koter, A. 2003, A&A, 404, 35
Min, M., Hovenier, J. W., & de Koter, A. 2005, A&A, 432, 909
O'Connell, D. J. K. 1933, Harvard Bull., 893, 14
Savage, B. D., & Mathis, J. S. 1979, ARA&A, 17, 73
Servoin, J. L., & Piriou, B. 1973, Phys. Stat. Sol. (b), 55, 677
Shenton, M., Evans, A., Albinson, J. S., et al. 1994, A&A, 292, 102
Sloan, G. C., & Price, S. D. 1995, ApJ, 451, 758
Spitzer, W. G., & Kleinman, D. A. 1960, Phys. Rev., 121, 1324
Tubbs, R. N., Meisner, J. A., Bakker, E. J., & Albrecht, S. 2004, in New Frontiers in Stellar Interferometry, Proc. SPIE, 5491, ed. W. A. Traub., Bellingham, WA: The International Society for Optical Engineering, 588
van Boekel, R. 2004, Ph.D. Thesis, University of Amsterdam
van Boekel, R., Min, M., Leinert, C., et al. 2004, Nature, 432, 479
van Boekel, R., Min, M., Waters, L. B. F. M., et al. 2005, A&A, 437, 189
Van Winckel, H. 2003, ARA&A, 41, 391
Van Winckel, H., Mathis, J. S., & Waelkens, C. 1992, Nature, 356, 500
Van Winckel, H., Waelkens, C., & Waters, L. B. F. M. 1995, A&A, 293, L25
Van Winckel, H., Waelkens, C., Fernie, J. D., & Waters, L. B. F. M. 1999, A&A, 343, 202
Verhoelst, T. 2005, Ph.D. Thesis
Voûte, J. 1940, Lembang Ann., 8, 42
Waelkens, C., Lamers, H. J. G. L. M., Waters, L. B. F. M., et al. 1991a, A&A, 242, 433
Waelkens, C., Van Winckel, H., Bogaert, E., & Trams, N. R. 1991b, A&A, 251, 495
Waters, L. B. F. M., & Waelkens, C. 1998, ARA&A, 36, 233
Waters, L. B. F. M., Trams, N. R., & Waelkens, C. 1992, A&A, 262, L37
Waters, L. B. F. M., Waelkens, C., Mayor, M., & Trams, N. R. 1993, A&A, 269, 242
Waters, L. B. F. M., Molster, F. J., de Jong, T., et al. 1996, A&A, 315, L361